JOURNAL OF Materials CHEMISTRY

Preparation and crystal structure of a new Sr containing sialon phase $Sr_2Al_xSi_{12-x}N_{16-x}O_{2+x}$ ($x \approx 2$)

Zhijian Shen,[a] Jekabs Grins,[a]* Saeid Esmaeilzadeh[a] and Helmut Ehrenberg[b]

[a]*Department of Inorganic Chemistry, Arrhenius Laboratory, Stockholm University, SE–106 91 Stockholm, Sweden*
[b]*Darmstadt University of Technology, Petersenstr. 23, D-64287 Darmstadt, Germany*

Received 26th October 1998, Accepted 5th February 1999

A nitrogen-rich sialon phase containing Sr or Eu, named the S-phase, has been reported to form in the M′–Si–Al–O–N systems with M′ = Sr and Eu. A sample with overall composition $Sr_2Al_{2.5}Si_{10}O_4N_{14.5}$ hot-pressed at 1800 °C for 2 h contained approximately 85 vol% of the S-phase, and in addition the α- and β-sialon phases and an amorphous phase. Its structure was solved from X-ray synchrotron powder data ($\lambda = 1.1608$ Å), using direct methods, and was refined by the Rietveld method from 131 reflections in the 2θ range 10–59° to $R_F = 2.7\%$, with the assumed composition $Sr_2Al_2Si_{10}O_4N_{14}$, space group *Imm*2, $a = 8.2788(9)$, $b = 9.5757(9)$, $c = 4.9158(4)$ Å, $V = 389.7$ Å^3. The structure model was confirmed by its electron diffraction pattern and by high-resolution electron microscopy studies. The structure exhibits a tetrahedral network with high connectivity, each tetrahedron sharing corners with seven surrounding tetrahedra, and the Sr atoms, irregularly coordinated by eight O/N atoms, are found in tunnels extending along [001].

Introduction

Nitrogen-rich sialon phases have attracted great interest, especially β-sialon $Si_{6-z}Al_zO_zN_{8-z}$ and α-sialon $M'_xSi_{12-(m+n)}Al_{(m+n)}O_nN_{16-n}$, in connection with the development of high-performance ceramic materials. Phase formation conditions and phase compatibility relationships have therefore been systematically determined in many M′–Al–Si–O–N systems, *e.g.* with M′ = Ca, Y, and rare-earth elements.[1] Less attention has been paid to the Sr-containing sialon system, most probably because of the common belief that Sr^{2+} with an ionic radius of 1.13 Å, like other cations with radii >1 Å, is too large to enter into the interstices of the α-sialon structure. This implies that structural restrictions should prevent formation of the α-sialon phase in this system.[2,3] It has lately become clear, however, that this is not a valid explanation. The formation/stability of an α-sialon phase is more likely to depend strongly on the phase compatibility relationships in the system in question rather than exclusively on the radius of the cation. We have for instance shown that the formation of the JEM-phase, $ReAl(Si_{6-z}Al_z)N_{10-z}O_z$, competes with that of α-sialon in Ce-, La-, Nd- and Sm-doped sialon systems.[4]

Until recently, no structural data of any Sr-containing sialon phase could be found in the literature. Lately, however, the structures of the two new compounds $Sr_2Si_5N_8$ and $SrSiAl_2O_3N_2$ were reported.[5,6] They were prepared by a novel synthesis technique, namely by reacting silicon diimide with metallic strontium, aluminium nitride and strontium carbonate under N_2 atmosphere in a high-frequency furnace at 1650 °C. In a recent study we found that two new phases were formed together with α- and β-sialon in Eu and Sr-doped systems.[7] One of these, the S-phase, was originally noticed by Hwang *et al.* in connection with their attempts to prepare α-sialon in the Si_3N_4–SrO–AlN system, but it was not structurally characterized, and its composition was not determined.[8] In the Sr sialon system the S-phase was found to co-exist with α- and β-sialon and a second Sr-containing phase. The structure and composition of the latter phase are presently under investigation. Our studies have so far shown that it is structurally similar to the sialon polytypoid phases.

The composition of the S-phase, as revealed by elemental analysis performed in a scanning electron microscope (SEM) using an energy-dispersive spectrometer (EDS), was found to be significantly different from those of the coexisting phases, which all contain considerably less Sr. So far we have not been able to prepare any phase pure S-phase sample, but an 85 vol% phase-pure specimen has been obtained by reacting appropriate amounts of Si_3N_4, AlN and $SrCO_3$. In this article we report on the preparation of the Sr S-phase and on its structure determination and refinement by the Rietveld method, based on synchrotron X-ray powder diffraction (XRPD) data. The compatibility relationships between this S-phase and its neighboring phases will be discussed in a forthcoming article.[9]

Experimental

The cation ratio in the S-phase was initially determined by SEM/EDS analysis of crystals in a sample with the nominal composition $Sr_{0.6}Al_{2.4}Si_{9.6}O_{1.2}N_{14.8}$, which had been hot-pressed at 1800 °C for 2 h and which contained the α- and β-sialon phases and the Sr-doped sialon polytypoid phase (see above) besides the S-phase. A series of specimens were subsequently prepared with cation ratios equal to that determined for the S-phase but with varying O/N atomic ratios. One specimen which contained more than 85 vol% S-phase, with α- and β-sialon as secondary phases, had the nominal composition $Sr_2Al_{2.5}Si_{10}O_4N_{14.5}$. This sample was prepared from an appropriate mixture of powders of Si_3N_4 (UBE, Tokyo, SN-E10), AlN (H.C. Starck, Berlin, grade A), and $SrCO_3$ (99.0%, Allied Chemical, NY, USA). Corrections were made for the oxygen present in the Si_3N_4 and AlN raw materials, corresponding to 2.7 and 1.9 wt% SiO_2 and Al_2O_3, respectively. The precursor powders were ball-mixed in water-free propanol for 24 h. The dried powder mixture was then hot-pressed at 1800 °C for 2 h under 35 MPa pressure in a graphite resistance furnace and in a nitrogen atmosphere.

The prepared sample was characterized by XRPD, both with a STOE STADI/P X-ray diffractometer operated in symmetric transmission mode and with a Guinier–Hägg camera, using strictly monochromatized Cu-Kα_1 radiation in both cases. Its microstructure was examined in a JEOL JSM 880 SEM equipped with an EDS.

High-resolution electron microscopy (HREM) images were recorded with a transmission electron microscope (TEM)

JEOL 3010, operated at 300 kV and with an optimal resolution of 1.7 Å. The HREM images were corrected for astigmatism and Fourier filtering was applied with the computer program CRISP.[10] Theoretical images for different crystallite thickness and defocus values were calculated with the program NCEMSS.[11]

Synchrotron powder diffraction data were recorded at the beamline B2 of HASYLAB, Hamburg (Germany), situated at a bending magnet of the storage ring DORIS. Photons with a wavelength of 1.1608 Å were selected with a Ge(111) double-crystal monochromator. Intensity data were measured with a scintillation NaI counter in Debye–Scherrer mode for a rotating capillary with a diameter of 1 mm, covering the 2θ range 5–70° in steps of 0.01°. To allow for the detection of radiation damage during the experiment, two successive runs were compared and were simply added together since no significant change was observed in the patterns.

Results and discussion

Microstructure

An SEM back-scatter electron image from a polished and carbon-coated surface of the sample with overall nominal composition $Sr_2Al_{2.5}Si_{10}O_4N_{14.5}$ is shown in Fig. 1. The Sr S-phase grains appear light gray and have sizes between *ca.* 2 and 10 μm. The elongated black grains are β-sialon, the small entrapped gray phase is α-sialon, and the light area with irregular morphology represents an amorphous phase. It can be noted that smaller crystallites of α- and β-sialon seem to have formed inside the grains of the S-phase

Structure determination and refinement

The powder pattern of the S-phase was indexed with an orthorhombic *I*-centered cell, using the TREOR90 version of the indexing program TREOR.[12] The obtained cell dimensions were $a=8.2788(9)$, $b=9.5757(9)$, $c=4.9158(4)$ Å, $V=389.70$ Å^3, using Al ($a=4.0494$ Å, JCPDS No. 4–787) as internal standard and 46 reflections for $2\theta<76°$. The indexed pattern is given in Table 1 for the first 20 observed lines.

No systematic absences could be observed in the powder pattern, except those due to the centering of the cell, indicating 5 possible space groups. The structure was solved by direct methods, using the program EXPO,[13] assuming a cell content of $Sr_2Si_{12}N_{18}$ and trying out different space-group possibilities. A satisfactory solution, with reasonable interatomic distances and R_F value, was obtained in space group *Imm*2 (no. 44).

The obtained structural model was refined using the GSAS program package,[14] the synchrotron XRPD data and 131 theoretical reflections for the S-phase in the 2θ range 10–59°. A total of 60 variables were used, including 14 positional and 6 thermal displacement parameters for the S-phase. A

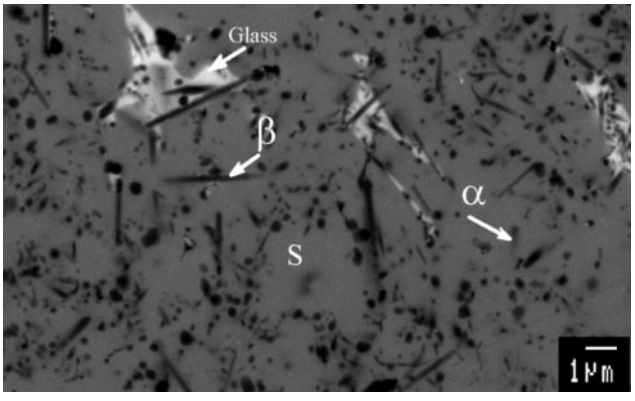

Fig. 1 SEM back-scatter electron image of an Sr sialon sample with nominal composition $Sr_2Al_{2.5}Si_{10}O_4N_{14.5}$.

Table 1 Observed and calculated 2θ values for the Guinier–Hägg diffraction pattern of $Sr_2Al_2Si_{10}N_{14}O_4$ up to the 20th observed line. $\Delta2\theta=2\theta_{obs.}-2\theta_{calc.}$. $\lambda=1.5406$ Å. Cell figure-of-merit: $M_{20}=54$, $F_{20}=75$ (0.0123, 22)

h	k	l	$2\theta_{obs}$/degrees	$\Delta2\theta$	d_{obs}/Å	I/I_0
0	2	0	18.533	0.017	4.784	2
0	1	1	20.302	0.012	4.371	8
1	0	1	21.001	0.003	4.226	15
2	0	0	21.449	0.032	4.133	2
1	2	1	28.148	0.009	3.168	19
2	2	0	28.491	0.009	3.130	12
2	1	1	29.691	−0.002	3.006	100
1	3	0	29.976	−0.004	2.979	65
0	3	1	33.452	0.007	2.667	15
3	1	0	33.752	−0.023	2.653	5
0	0	2	36.534	0.005	2.4575	17
3	0	1	37.363	0.024	2.4049	4
0	4	0	37.562	0.021	2.3926	2
1	1	2	39.348	−0.001	2.2880	16
2	3	1	40.104	0.025	2.2466	1
0	2	2	41.257	0.003	2.1864	9
3	2	1	41.982	−0.006	2.1504	28
2	0	2	42.768	0.016	2.1126	4
1	4	1	43.408	0.002	2.0829	9
4	0	0	43.676	−0.024	2.0708	12

Debye–Scherrer absorption correction with $\mu R=1.2$ was applied, and the β- and α-sialon phases present in the sample were included in the refinement with atomic coordinates from ref. 15 and 16, respectively. The refinement converged with $wR_p=6.3\%$, $R_p=4.8\%$, $\chi^2=2.5$ and $D_{wd}=0.86$. The corresponding R_F values were 2.7% for the S-phase, 3.5% for the β-sialon (59 reflections) and 6.6% for the α-sialon phase (100 reflections). The fit between observed and calculated intensities is illustrated in Fig. 2. The refined weight fractions of the β- and α-sialon phases were 8.6(3) and 5.0(2)%, respectively. The refined unit cell parameters for the β-sialon were $a=7.6129(3)$, $c=2.9140(2)$ Å, yielding an estimate of $z=0.3$ in $Si_{6-z}Al_zO_zN_{8-z}$. The refined value of the site occupancy factor for Sr in the α-sialon phase was 0.08(1).

The final atomic coordinates for the S-phase are given in Table 2. The unit cell was found to contain 2 Sr, 12 M = (Si,Al) and 18 X = (N,O) atoms. A postulated composition of the phase with no Al in it is accordingly $Sr_2Si_{12}N_{16}O_2$. The EDS analysis results clearly show, however, that the phase contains Al and has a composition around $Sr_2Al_2Si_{10}N_{14}O_4$ or $Sr_2Al_xSi_{12-x}N_{16-x}O_{2+x}$ ($x\approx2$). As expected, the distribution of the Al and O atoms in the structure could not be discerned from the present X-ray data reflection intensities. A plausible distribution of the Al and O atoms on the available sites can, however, be inferred from the observed interatomic distances. The M atoms are found to occupy one 4(d) site

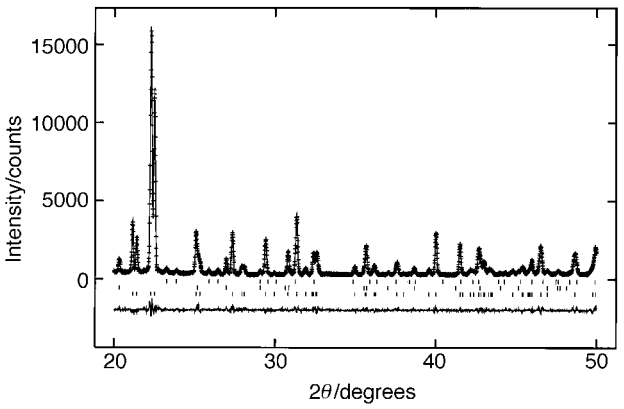

Fig. 2 Observed (crosses), calculated (solid line) and difference (bottom) XRPD pattern of Sr S-phase $Sr_2Al_xSi_{16-x}N_{14-x}O_{2+x}$ ($x\approx2$) for $2\theta=20$–50° ($\lambda=1.1608$ Å).

Table 2 Atomic coordinates for $Sr_2Al_2Si_{10}N_{14}O_4$; orthorhombic, $a=8.2788(9)$ Å, $b=9.5757(9)$ Å, $c=4.9158(4)$ Å, *Imm*2, $Z=1$

Atom	Site	x	y	z	$U/100$ Å^2	s.o.f (site occupancy fraction)
Sr	2(a)	0	0	0.2660(4)	6.93(7)	
Si	4(d)	0	0.3381(3)	0.6526(6)	2.27(6)	
(Si,Al)	8(e)	0.8085(2)	0.3354(2)	0.1575(5)	2.14(4)	25% Al, 75% Si
(N,O)	4(c)	0.7347(6)	1/2	0.1356(10)	2.1(2)	50% O, 50% N
O	2(b)	0	1/2	0.5749(11)	2.8(2)	
N1	8(e)	0.8301(5)	0.2746(5)	0.4958(7)	2.0(1)	
N2	16(f)	0	0.3073(7)	0.0003(11)	1.6(2)	

Table 3 Bond distances (Å) for $Sr_2Al_2Si_{10}N_{14}O_4$

Sr–(N,O) $2\times2.660(5)$	Si–O 1.597(3)	(Si,Al)–(N,O) 1.694(2)
N1 $4\times3.189(5)$	N1 $2\times1.715(4)$	N1 1.749(5)
N2 $2\times3.219(7)$	N2 1.734(6)	N1 1.771(4)
		N2 1.784(3)
	mean 1.69	mean 1.75
	expected 1.71	expected 1.75
(N,O)–(Si,Al) $2\times1.694(2)$	N1–Si 1.715(4)	N2–Si 1.734(6)
Sr 2.660(5)	(Si,Al) 1.749(5)	(Si,Al) $2\times1.784(3)$
	(Si,Al) 1.771(4)	Sr 3.219(7)
O–Si $2\times1.597(3)$	Sr 3.189(5)	

and one 8(e) site. The mean metal–anion distance is found to be longer at the 8(e) site (see Table 3), and we therefore conclude that the Al resides on this site and that it is occupied by both Al and Si atoms in the ratio 1 : 3. The X atoms occupy one 2(b), one 4(c), one 8(e) and one 16(f) site. The anion on the 2(b) site is coordinated only by two M atoms, and we assume this site to be occupied only by O atoms. The anions on the 8(e) and 16(f) sites are coordinated by three M atoms and one Sr atom and are thus concluded to be N atoms. The 4(c) site is accordingly, assuming the composition $Sr_2Al_2Si_{10}N_{14}O_4$, occupied by both N and O atoms in the ratio 1 : 1.

Structure description

Selected bond distances are given in Table 3 together with expected M–X distances calculated from effective ionic radii in nitrides[17] of $N^{3-}(III)=1.44$ Å, $N^{3-}(II)=1.42$ Å, $Si^{4+}(IV)=0.29$ Å, $Al^{3+}(IV)=0.41$ Å, and effective ionic radii for oxygen ions[18] of $O^{2-}(III)=1.36$ Å, $O^{2-}(II)=1.35$ Å. The Si (site 4(d)) and M = (Si,Al) (site 8(e)) atoms are tetrahedrally coordinated by X = (N,O) atoms. The tetrahedral $M_{12}X_{18}{}^{4-}$ framework is illustrated in Fig. 3. The framework contains interconnected two-membered chains of (Si,Al)–(Si,Al) and (Si,Al)–Si tetrahedra along [001]. The connectivity is high, each tetrahedron sharing corners with seven surrounding tetrahedra. The anions at $y=0$ and 1/2, assumed in the refinement to be predominantly oxygen atoms, connect two tetrahedra; and those at $y\approx1/4$ and 3/4, assumed to be nitrogen atoms, three tetrahedra. The Sr atoms, irregularly coordinated by eight X atoms at an average distance of 3.07 Å, are found in tunnels extending along [001]. The observed average Sr–X distance is longer than an expected Sr(VIII)–N distance of *ca.* 2.7 Å, which may explain the comparatively high thermal displacement factor for Sr. The coordination of the X atoms by metal atoms may be summarized as: O by 2 Si atoms at 1.597(3) Å; (N,O) by 2 (Si,Al) atoms at 1.694(2) Å and 1 Sr at 2.660(5) Å; N1 by 3 (Si,Al) atoms at an average of 1.745 Å and 1 Sr at 3.189 Å; and N2 by 3 (Si,Al) atoms at an average of 1.767 Å and 1 Sr at 3.219 Å.

High-resolution electron microscopy

Electron diffraction patterns of the S-phase confirmed the *I*-centered unit cell obtained from the X-ray powder data. An HREM image of the S-phase along the [001] zone axis is shown in Fig. 4(a). The image contrast changes due to varying crystal thickness and vertical position. An image which is Fourier filtered and corrected for astigmatism is shown in Fig. 4(b). In order to test how well the experimental HREM image fits the derived structural model, a series of images were calculated using the atomic coordinates obtained from the structure refinement. A calculated image, for a thickness of 50 Å and a defocus of 900 Å, is inserted in Fig. 4(b) to show the agreement with the observed image. The structure of the S-phase can be recognized in the calculated image with the Sr atoms observed as white dots in a centered array and each Sr atom surrounded by a compressed hexagon of $(Si,Al)(O,N)_4$ tetrahedra.

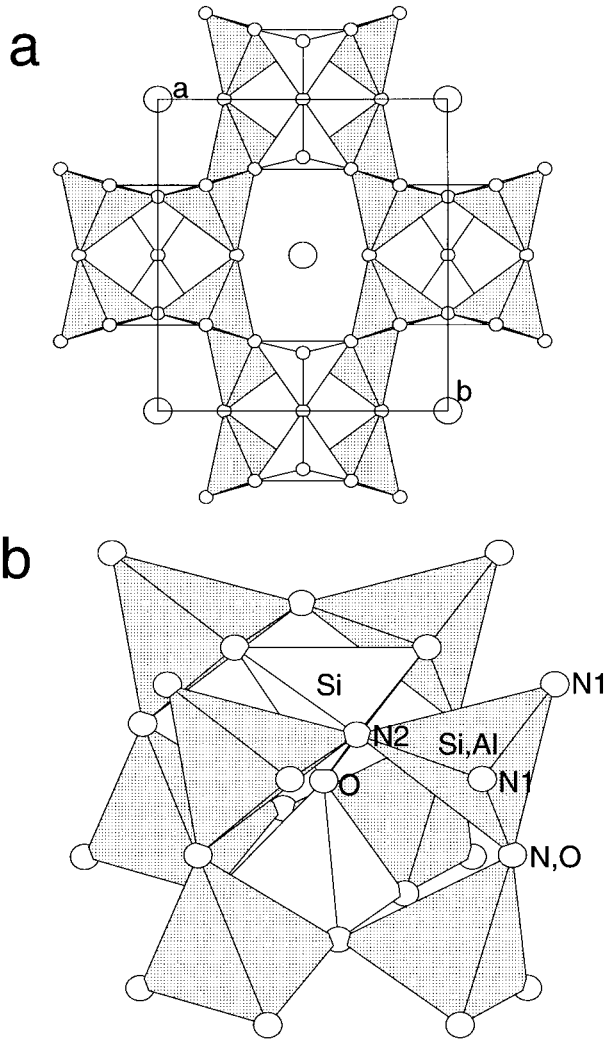

Fig. 3 (a) Illustration of the tetrahedral framework of the S-phase structure projected on the (110) plane. The positions of the Sr atoms are shown by unfilled circles. (b) Illustration of a part of the interconnected two-membered chains of tetrahedra extending along [1/2 0 z].

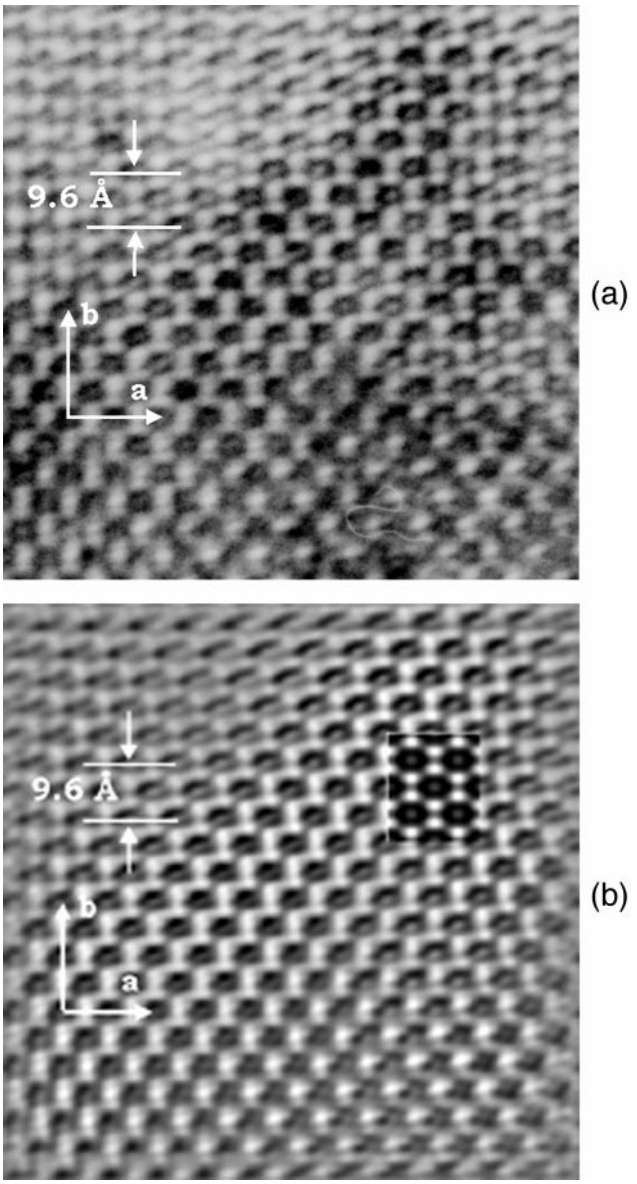

Fig. 4 (a) Observed HREM image of the Sr S-phase along [001]. (b) A corresponding observed HREM image which is Fourier filtered and corrected for astigmatism. The insert shows a calculated image for a crystal thickness and defocus value of 50 and 900 Å, respectively.

Concluding remarks

In this article we have described the preparation and crystal structure of $Sr_2Al_xSi_{12-x}N_{16-x}O_{2+x}$ with $x \approx 2$, which is seemingly isotypic with the previously reported S-phase. So far we have not been able to prepare monophasic samples, and accordingly we have not been able to investigate to what extent this phase can have a variable Si to Al content. Our studies of the Eu-doped sialon system has revealed that the S-phase also occurs in this system.[7] It is, however, even more difficult to obtain phase-pure samples in this system, partly because Eu^{3+} must first be reduced to Eu^{2+} when using Eu_2O_3 as precursor oxide, before the S-phase can be formed. We have, however, been able to calculate the unit cell parameters of the Eu-containing S-phase and found them to be $a=8.207(1)$, $b=9.537(1)$, $c=4.9038(6)$ Å.

The structure of the S-phase illustrates well one main difference between the crystal chemistry of nitridosilicates and oxosilicates.[19] Oxygen atoms in the structures of the latter are normally part of an SiO_4 tetrahedron and are usually bound either terminally or as bridging atoms to two neighboring Si atoms. An SiO_4 tetrahedron can in that case be connected, *via* corner-sharing, to up to four surrounding tetrahedra. In contrast, the N atoms in nitridosilicates can link up to four SiN_4 tetrahedra, allowing a higher connectivity in the network.

Acknowledgement

The authors thank Professor M. Nygren for support and valuable discussions.

References

1 T. Ekström and M. Nygren, *J. Am Ceram. Soc.*, 1992, **75**, 259.
2 D. Stultz, P. Greil and G. Petzow, *J. Mater. Sci. Lett.*, 1986, **5**, 335.
3 K. H. Jack, in *Progress in Nitrogen Ceramics*, ed. F. L. Riley, Nijhoff, The Hague, Netherlands, 1983, pp. 45–60.
4 J. Grins, Z. J. Shen, M. Nygren and T. Ekström, *J. Mater. Chem.*, 1995, **5**, 2001.
5 T. Schlieper, W. Milius and W. Schnick, *Z. Anorg. Allg. Chem.*, 1995, **621**, 1380.
6 R. Lauterbach and W. Schnick, *Z. Anorg. Allg. Chem.*, 1998, **624**, 1154.
7 Z. J. Shen, M. Nygren, P. Wang and J. Feng, *J. Mater. Sci. Lett.*, 1998, **17**, 1703.
8 C. J. Hwang, D. W. Susnitzky and D. R. Beaman, *J. Am. Ceram. Soc.*, 1995, **78**, 588.
9 Z. J. Shen, J. Grins, S. Esmaeilzadeh and M. Nygren, to be presented at *6th Conference of Eur. Ceram. Soc.*, *June*, *1999*, *UK.*
10 S. Hovmöller, *Ultramicroscopy*, 1192, **41**, 121.
11 M. A. O'Keefe and R. Kilaas, *Users Guide to NCEMSS*, National Center for Electron Microscopy, Materials Science Division, Lawrence Berkely Laboratory, University of California, 1994.
12 P.-E. Werner, L. Eriksson and M. Westdahl, *J. Appl. Crystallogr.*, 1985, **18**, 367.
13 A. Altomare, M. C. Burla, G. Cascarano, C. Giacovazzo, A. Guagliardi, A. G. G. Moliterni and G. Polidori, *J. Appl. Crystallogr.*, 1995, **28**, 842.
14 A. C. Larson and R.B. Von Dreele, Los Alamos National Laboratory Report No. LA-UR-86-748, 1987.
15 R. Grün, *Acta Crystallogr.*, *Sect. B*, 1979, **35**, 800.
16 F. Izumi, M. Mitomo and Y. Bando, *J. Mater. Sci.*, 1984, **19**, 1984.
17 W. H. Bauer, *Cryst. Rev.*, 1987, **1**, 59.
18 R. D. Shannon, *Acta Crystallogr.*, *Sect. A*, 1976, **32**, 751.
19 H. Huppertz and W. Schnick, *Chem. Eur. J.*, 1997, **3**, 249.

Paper 8/08256A